Photonics and Nanostructures - Fundamentals and Applications 55 (2023) 101154

Contents lists available at ScienceDirect

Photonics and Nanostructures - Fundamentals and Applications

journal homepage: www.elsevier.com/locate/photonics

Theoretical analysis of composite nanostructure with three-dimensional photonic lattice for ultra-broadband and polarization-independent absorption

Yang Li [a], Jinghao Wu [a], Yan-Long Meng [a,b,*], Yi Li [a], Yan-Song Li [a], Guiming Pan [a], Juan Kang [a], Chunlian Zhan [a], Zidong Wang [a], Shitao Hu [a], Shang-Zhong Jin [a]

[a] College of Optical and Electronic Technology, China Jiliang University, Zhejiang 310018, China
[b] State Key Laboratory of Applied Optics, Changchun Institute of Optics, Fine Mechanics and Physics, Chinese Academy of Sciences, China

ARTICLE INFO

Keywords:
Absorption
Ultra-broadband
Nanostructure
Photonic lattice
Three-dimensional

ABSTRACT

In this study, we present a composite nanopillar array with an average absorption efficiency near 100% in an ultra-broad wavelength range from 300 nm to 2000 nm. In particular, the average absorption in the band range from 400 nm to 1000 nm is close to 99% due to the strong coupling between the composite nanopillars and a complementary absorption generated by the two kinds of nanopillars in one period. The real and imaginary parts of the absorber's impedance present a fluctuation near 1 and 0 in the entire wavelength range, which indicates an ultra-weak reflection of the absorber. The device also shows insensitivity to the polarization state and angle of incidence. The research offers a novel strategy for achieving high-efficiency light absorption in an ultra-broad wavelength range and boosts the potential value of composite nanostructures for thermophotovoltaic cells, electromagnetic stealth, and stray light suppression.

1. Introduction

Since it can modulate the incident electromagnetic waves with large freedom by designing the structure elaborately according to the demands[1], metamaterials have been extensively studied in many application fields, such as high-performance directional radiation antennas[2,3], electromagnetic stealth[4,5], space communication[6,7], and selective absorbers. Especially for the application in electromagnetic absorption, which can be widely used in electromagnetic stealth, low-noise space light detection, and solar energy utilization, metamaterials present immense advantages. In 2008, the Landy team[8] proposed the first metamaterial resonator metamaterial structure, and in the frequency range of 11–12 GHz, the selective absorber achieved an absorption close to 100% at the target wavelength range. Up to now, metamaterial absorbers have drawn a growing amount of attention to unearthing their application potential. Yang's team developed a square ring-metal wire structure-based optically excited, dynamically switchable dual-frequency terahertz metamaterial absorber. Li's team developed a three-dimensional metamaterial structure-based absorber that achieved over 90% absorption in the 356–737 THz range. A metal column array-based absorber with high absorption in the frequency range of 1.5–3 THz was proposed by Nejat's team[9–11]. The study of metamaterial perfect absorbers that can cover the visible and infrared bands has more practical value for enhancing the performance of solar energy-based energy devices than selective absorbers, which have been the focus of research on selective absorbers in addition to applications in the terahertz and infrared bands.

To extend the absorption bandwidth of the absorber for absorbing solar energy, Cong and Hoa [12,13]designed a metal/dielectric multilayer stacked absorber based on Au/Si material. The absorption band of the 5-layer stacked structure is 400–750 nm, while the absorption band of the 10-layer stacked structure is 480–1480 nm. Wu et al. [14] designed a hyperbolic metamaterial absorber using W/SiO_2, which can extend the absorption band to 260–1580 nm with an average absorption rate of 98.9%. Yi et al. [15]proposed a W/SiO_2 four-layer disc structure, which achieved over 90% absorption in the 420–1950 nm band. To expand the absorption band edge from visible to near 3000 nm, several teams coupled specific top layer structures with dielectrics to achieve high absorption over a wide band. By introducing a metal layer in the dielectric structure, excellent light trapping can be achieved by surface

* Corresponding author at: College of Optical and Electronic Technology, China Jiliang University, Zhejiang 310018, China.
E-mail address: myl@cjlu.edu.cn (Y.-L. Meng).

https://doi.org/10.1016/j.photonics.2023.101154
Received 8 March 2023; Received in revised form 26 April 2023; Accepted 14 May 2023
Available online 24 May 2023

plasmon excitations, which can enhance the absorbance of the structure [16,17]. As a heat-resistant material, titanium shows high mechanical stability and a large imaginary part of its dielectric constant. The large imaginary part of the dielectric constant means an electromagnetic solid loss. Accordingly, Ti was widely used in absorbers for realizing good light absorption over a wide wavelength range[18]. Qin reported an absorber, of which the efficiency reached 90% over a broad wavelength range from 300 nm to 3000 nm by utilizing a Ti thin film and a nanopillar array composed of TiN and SiO_2. The reported absorber was also insensitive to the polarization of light[19]. So far, studies using hole arrays[20], complementary crosses and cylinders[21], and multilayer structures[22] have emerged to achieve high-efficiency absorption.

To obtain a strong absorption in an ultrabroad wavelength range, this paper proposed an absorber with two kinds of composite nanopillar array, of which the bottom materials are TiN and TiO_2, respectively. Both kinds of nanopillars are stacked with different materials. The radius of the nanopillars and the thickness of each layer in the nanopillar keep the same. This hybridization breaks the symmetry of the conventional structure and not only broadens the bandwidth of the absorbing structure but also improves the absorption of the metamaterial structure to a certain extent. This structure has an average absorption of more than 97% from 300 nm to 2000 nm in the wavelength range. In the wavelength range from 400 nm to 1000 nm, the absorption can reach 99% evenly. The nanopillar array is designed on the top of a thick TiN, ensuring no light can pass through the absorber. In addition, the impedance matching of the structure and the effect of different top materials, bottom materials, and material thickness on absorption are studied carefully in this chapter. The results confirm the effectiveness of the structure. The insensitivity of the structure to polarization was also demonstrated by varying the light incidence as well as the angle of polarization. The proposed metamaterial multilayer material composite nanopillar structure with a thickness of 300 nm is realized to minimize the reflectivity by designing the permittivity and permeability of the structure using impedance-matching in free space. This research is expected to promote the development of ultra-broadband, high-efficiency Lambertian absorber structures, which are of great importance for applications in clean energy, scattered light suppression, and electromagnetic stealth based on solar light absorption.

2. Simulation model

As shown in Fig. 1, a nanocolumn periodic array composed of multiple layers of materials is arranged on the surface of the TiN layer. The nanocolumn array includes two types of nanocolumns with the same period but different materials. The bottom materials of the two types of nanocolumns are TiO_2 and TiN, with thicknesses of L_{51} and L_{52}, respectively. Titanium nitride is a well-known refractory material, which is also widely used in various absorbing structures as a plasmonic material for substituting those noble metals to generate strong plasmon resonance in visible and near-infrared bands[23]. Titanium oxide, as a titanium-based material, also has high-temperature resistance. In the visible light range, titanium dioxide has a high refractive index, while its absorption ability is weak in the near-infrared band. When the two materials are combined, the optical properties of the composite film can be adjusted by changing the physical parameters of the structure, thereby enhancing the absorption ability of the device. From bottom to top, all other layers including Ti, GaP, SiO_2, and GaAs are made of the same thickness, denoted as L_1, L_2, L_3, and L_4, respectively. All nanocolumns have the same height "H", radius "R", and period "T", which can simplify the processing size and etching time. Table 1 gives the specific parameters and initial values of the structural model used in this paper for simulation.

In this study, a Finite-Difference Time-Domain (FDTD) analysis method is used to calculated the reflectance, absorptive power density, and the distribution of electric field. As shown in Fig. 1(a), two types of composite nanopillars are set into one simulation period to forming a three-dimensional photonic lattice. The x and y-direction boundaries in the simulation region are set to periodic boundary conditions, while the z-direction boundary condition is defined as a perfect matching layer. The simulation environment is assumed to be atmospheric with a background index of 1. A plane wave is used as an excitation source with a spectral range from 300 nm to 2000 nm. The plane wave propagates along the negative direction of the z-axis and polarizes along the x-axis. The reflectivity data are obtained by a power monitor set above the exciting source. A 200 nm-thick TiN is used as a substrate to ensure that there is no light passing through. According to the principle of energy conservation, the device's absorption can be expressed as A= 1-R. All the optical constants of the materials used in the simulation are obtained from the PALIK database[24–28]. The refractive index and extinction coefficient of the materials are plotted in Fig. 2.

3. Results and discussion

Fig. 3 shows the absorption curves of the device using different metals as L_4 layer. It is obvious that the devices, of which the L_4 layers

Table 1
Summary of optimized structural parameters.

Layer Structural	Fixed-Parameter
Nanopillar array size	
L_1 = 4 nm	T = 256 nm,
L_2 = 60 nm	R= 112 nm
L_3 = 25 nm	H = 244 nm
L_4 = 110 nm	
L_{51}、L_{52} = 45 nm	

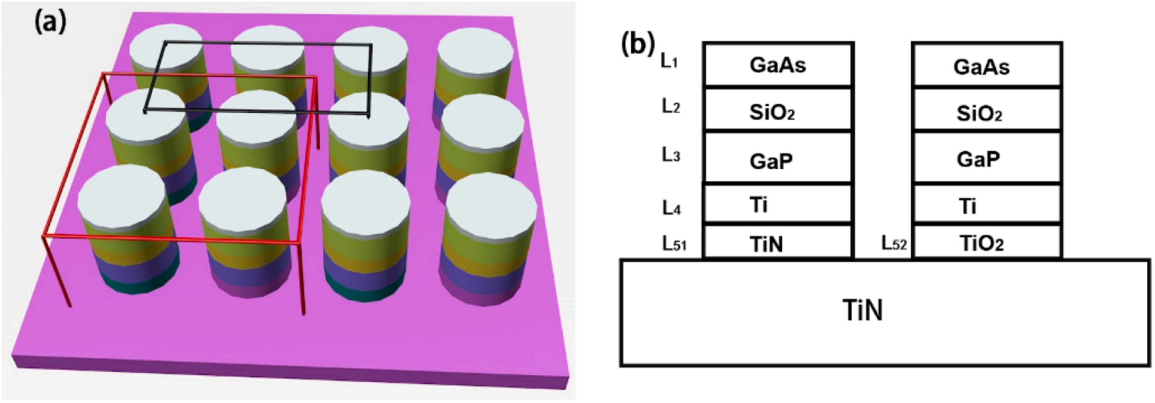

Fig. 1. (a) 3D image of the proposed structure. (b) Cross-section of the proposed absorber.

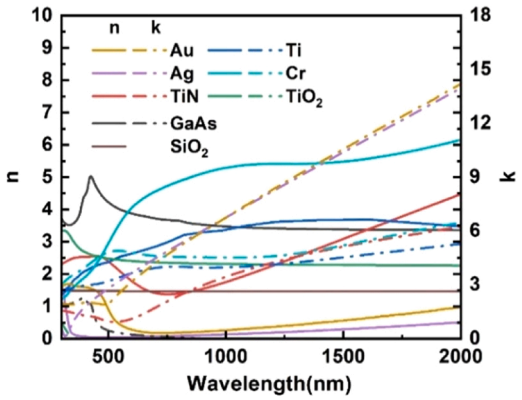

Fig. 2. Comparison of the optical constants of the materials used in the simulation.

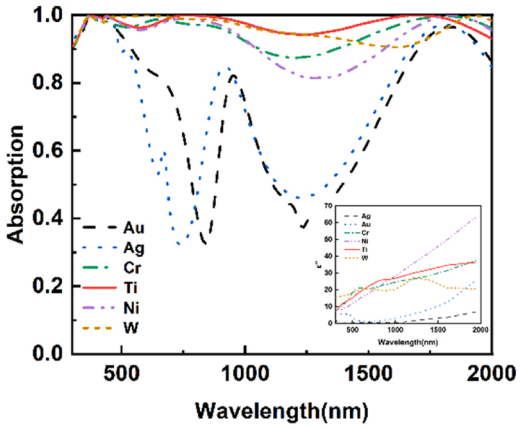

Fig. 3. Absorption curves of devices with different plasmonic materials and imaginary part of the dielectric constant of materials. Inset: Comparison of the imaginary parts of the metals' permittivities.

are Ti, Cr, Ni, and W, present a higher average absorptance in comparison with that based on the noble metals, such as Au and Ag. Among those devices, the device using Ti as L_4 layer shows the strongest absorptance than other devices in the wavelength range from 800 nm to 1700 nm. That because titanium not only has a strong intrinsic loss in the visible range, the surface plasmon is also helpful of enhancing the intensity of electric field nearby the surface by coupling with the opposite titanium layer in another nanopillar. Furthermore, titanium has a lower Q resonance that can excite a broader band response in the infrared region in comparison with those noble metals[29–31]. Although noble metals have strong SPR in the visible wavelength range, their plasmon resonance band is relatively narrow [32,33]. At last, the low imaginary part of permittivity (see the inset of Fig. 3) of these noble metals dominates the absorption which causes the absorption to decrease to 80% evenly in the wavelength range from 300 nm to 2000 nm. The worse absorption will lead to a strong loss of solar energy finally. In another hand, all those heat-resistant materials exhibit significant broad-band plasmon resonance behavior and have a high imaginary part of permittivity over a broad frequency range, as shown in the inset of Fig. 3. That leads to high absorption over a wide range of wavelengths[34–36]. As a result, The devices using different heat-resistant materials exhibit similar absorption in the 300–1000 nm range. However, the absorption of the device using Ti as the L_4 layer significantly increases since the wavelength exceeds 1000 nm. Therefore, titanium will be the best choice as the L_4 layer to broaden the device's absorption bandwidth effectively and improve its absorption capacity.

The L_3 layer of the device is made of gallium phosphide, with a thickness of 25 nm, and has excellent absorption properties for short-wavelength light sources[37]. GaAs thin film is an ideal intermediate layer for efficient absorption structures due to its excellent infrared transmission ability and outstanding mechanical properties. The L_2 Layer is made of SiO_2, with a thickness of 60 nm, and the good electrical properties of the oxide film can effectively suppress surface reflection, exhibiting strong anti-reflection ability. Moreover, SiO_2 can also play a role in phase and amplitude matching in the nanorod structure, enhancing the device's absorption capacity. The L_1 Layer is made of GaAs with a thickness of 4 nm. The addition of GaAs material increases the total absorption of the device from 93% to 98%. The bandgap of GaAs is 1.4 eV, so it can absorb visible and near-infrared light, and its absorption ability is particularly strong in the range of 400–500 nm[38]. However, the absorption of the device is greatly affected by GaAs with different thicknesses, as shown in Fig. 4(a). The parameters of the material are closely related to the performance of the device. In Fig. 4, the absorption of the structure is calculated by gradually changing the thickness of the material layer using the controlled variable method. It's a common method for device optimization. In Fig. 4(b), the increase in the thickness of the titanium layer gradually reduces the absorption of the device in the range of 1000–1700 nm. Moreover, the absorption peak in the long wavelength range continuously shifts towards the far-infrared wavelength region. Therefore, considering that the absorption band of the device must match the solar spectrum, the optimal thickness value of the Ti layer is determined to be 110 nm. In Fig. 4(c), the variation of the SiO_2 layer thickness plays a key role in the visible light absorption of the film, and an appropriate SiO_2 layer thickness can adjust the phase and amplitude of light, enhancing the overall absorption capacity of the device.

Table 2 shows a comparison between previously reported examples of ultra-broadband absorbers using refractory metals and the examples presented in this paper. The table lists the materials used in the absorber, the bandwidth of more than 90% absorption, and the average absorption. Li's triple-layered nanodisk array based on TiN can achieve about 90% absorption in the visible range of 400–800 nm[39]. Liu's multi-layered nanocolumn structure composed of TiN and TiO_2 can achieve over 90% absorption in the range of 400–1500 nm[40]. It is worth mentioning that the absorption bandwidth of the absorber proposed in this paper is 1700 nm, and the absorption exceeds 97%, highlighting the broadband absorption characteristics of the absorber. While designing the structure, the nanorod structure made of TiN material is insufficient to achieve high absorption. However, titanium dioxide, which is also a titanium-based material, can increase the overall absorption of the structure, as shown in Fig. 5. Titanium nitride has good plasma resonance characteristics, which can achieve higher absorption in short wavelengths. Transparent titanium dioxide films have high-temperature-resistant physical characteristics similar to those of titanium nitride. Although titanium dioxide has a higher refractive index in the visible light band, its absorption in the near-infrared is not ideal. However, by comparing the absorption curves of the two structures, we propose a hypothesis that when two types of nanorods made of different materials are arranged in an alternating pattern, the device may exhibit multiple optical properties due to the difference in refractive index and band gap of the two materials. Specifically, the optical properties will be affected by the physical parameters of the alternating structure. Therefore the overall absorption of the structure can be adjusted by modifying the physical parameters of the device. Thus, the hybrid nanorod structure can have absorption characteristics of both single nanorod structures, achieving higher absorption in the wavelength range of 300–2000 nm. To verify this hypothesis, we calculated the absorption and corresponding S parameters of the single nanorod structure and the mixed nanorod structure with alternating nanorods. Our research findings are presented in Fig. 5 and subsequent impedance analyses, comparing the absorption and impedance under three different conditions. As can be seen clearly from the absorption curve in Fig. 5, these

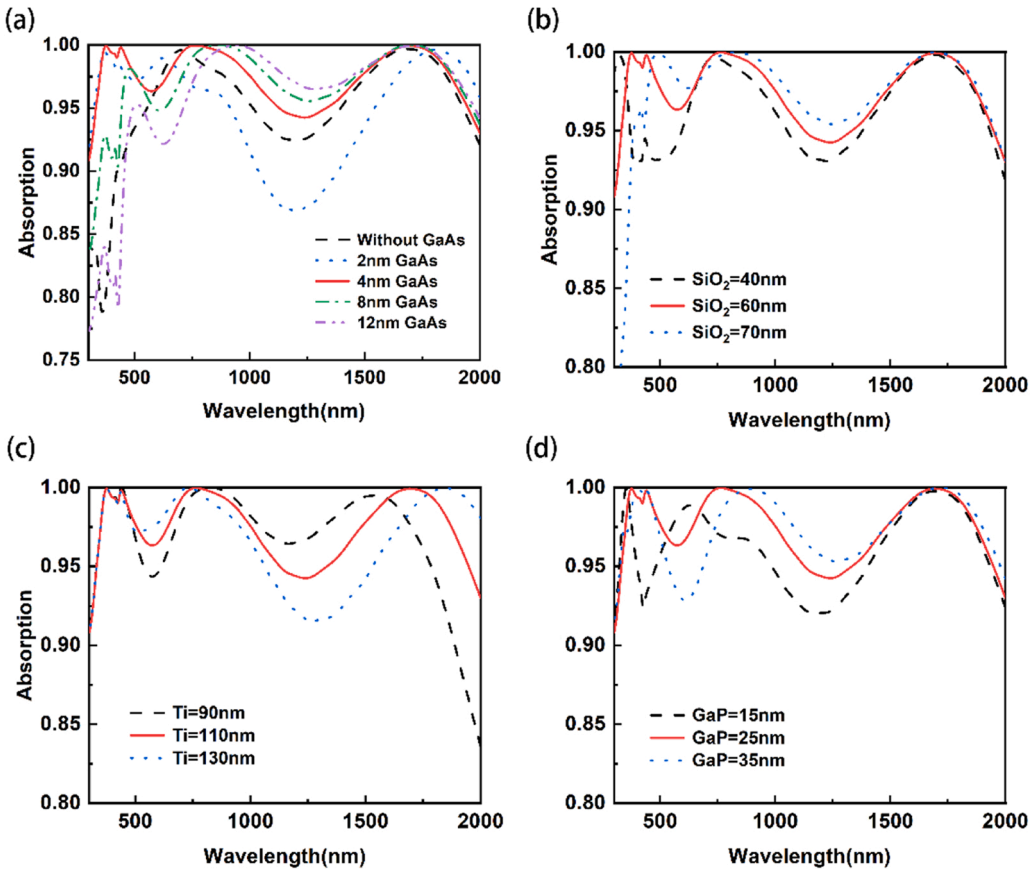

Fig. 4. Absorption curves of devices with different thicknesses of GaAs (a), SiO_2 (b), Ti (c), and GaP (d).

Table 2
Comparison between the different absorber designs proposed in previous studies.

Refs.	Metallic materials	Bandwidth (Absorption>90%)	Average absorption in this region
[39]	TiN/SiO_2	400–800 nm	> 90
[40]	TiN/TiO_2	300–1400 nm	> 90
[41]	Ni	300–1600 nm	95.77%
Our work	TiN/TiO_2/Ti	300–2000 nm	97.5%

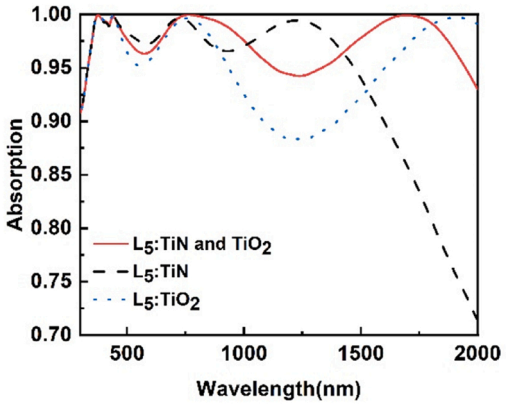

Fig. 5. Comparison of absorption among three structures.

three structures have more than 95% absorption in the low-wavelength range of 300–600 nm. However, as the wavelength increases, the absorption of the devices with different types of nanocolumns based on titanium nitride and titanium dioxide begins to decrease. The titanium nitride nanocolumn structure still has high absorption in the wavelength range of 1000–1500 nm, but its absorption rapidly decreases in the range of 1500–2000 nm. On the contrary, the titanium dioxide nanocolumn structure has low absorption in the range of 1000–1500 nm but shows high absorption in the range of 1500–2000 nm. Therefore, the device composed of two types of nanorods arranged in an alternating pattern exhibits complementary absorption behavior. The device demonstrates exceptional absorption performance across a wide wavelength range, verifying the hypothesis and highlighting the remarkable absorption capability of the hybrid nanorod structure and its potential as a promising candidate for various applications. Further research to optimize and expand this structure can improve its performance and broaden its applications, making it widely applicable in metamaterial absorption structures.

To further verify the hypothesis, we observed the modulation of absorption by changing some physical parameters of the device. As shown in Fig. 6, the thickness of the L_5 layer of the nanorods has an impact on the absorption of the device. Fig. 7 also demonstrates the modulation of the optical properties of the device by changing the period (T) and radius (R) of the nanorods. Interestingly, as the thickness of the L_5 layer increases, the optical properties of the device gradually approach those of a single TiO_2 nanorod, with absorption decreasing in the infrared range of 800–1700 nm. The absorption peak shifts towards the infrared region. Conversely, when the thickness of the L_5 layer decreases, the optical properties of the device approach those of a single TiN nanorod. Modulation of absorption can also be achieved by changing the radius and period of the nanorods, with absorption gradually decreasing in the near-infrared range as the radius increases from 112 nm to 115 nm and the period increases from 256 nm to 280 nm. These findings suggest that by designing structures with different optical properties using materials with varying optical properties, the desired

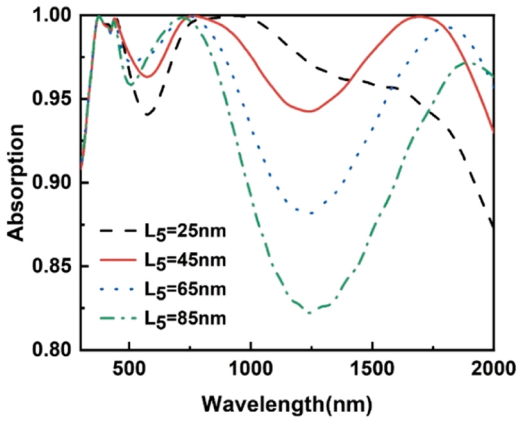

Fig. 6. Comparison of absorptance as the thickness of L_5 in the absorber changes from 25 nm to 85 nm.

optical properties of the device can be optimized. These ideas may provide new insights into future studies on light absorption and the development of various new materials.

Optical impedance matching is one of the more important methods used to analyze the absorption of metamaterial structures[42]. The relative impedance of the structure can be calculated by numerically simulating the scattering parameters. The relative impedance Z_r and reflectance[43,44] of the device when the incident light is incident perpendicularly to the surface of the metamaterial structure can be expressed, respectively, as :

$$Zr = \frac{Z(\omega)}{Z0} = \sqrt{\frac{(1+S11)^2 - S_{21}{}^2}{(1-S11)^2 - S_{21}{}^2}} \tag{1.1}$$

$$R(\omega) = \left|\frac{Z(\omega) - Z_0}{Z(\omega) + Z_0}\right|^2 \tag{1.2}$$

Where S_{11} and S_{21} denote the reflection and transmission scattering matrix coefficients of the normal incident light in TM polarization. $Z(\omega)$ is the impedance of the device and Z_0 is the impedance of the free space. Since the device substrate is 200 nm thick titanium nitride, resulting in almost no light passing through the structure, the parameter S_{21} can be set to zero. The relative impedance of an absorbing structure, as presented in Eq. (1.1), is an essential factor in achieving perfect absorption. When the structural impedance matches that of free space, indicated by a relative impedance of 1, perfect matching is achieved. The reflectance of the absorber is minimal, as described by Eq. (1.2), resulting in 100% perfect absorption. To further illustrate this point, Fig. 8 showcases the relative impedance curves of the proposed devices. The figure highlights that the device's relative impedance is close to 1 for the real part Re(Z_r) and 0 for the imaginary part Im(Z_r) throughout the waveband. This phenomenon signifies that the device's absorption rate is high. Notably, the real part of the relative impedance is close to 1, and the imaginary part is 0 at wavelengths of 1690 nm and 760 nm. These values correspond to a structure absorbance of 100%.

Figs. 8 and 9 show the impedance and absorption characteristics of three structures, and impedance matching analysis is performed on the absorption of the interleaved nanorods. As shown in Fig. 9, when L_5 is a single TiN or TiO_2 layer, the real and imaginary parts of the relative impedance of the structure are displayed. In the visible light wavelength range, the difference between the real and imaginary parts of the relative impedance is small, and the absorption of the single nanorod device is still high. However, as the wavelength increases, the real and imaginary parts gradually shift, the impedance-matching effect weakens, and the absorption significantly decreases. For the real and imaginary parts of the mixed nanorod impedance, similar changes to those of a single TiO_2 structure are observed. To achieve the goal of high absorption, the electromagnetic parameters of the L_5 layer of the mixed nanorod metamaterial structure, including permeability and conductivity, are optimized and adjusted to achieve matching between the structural impedance and spatial impedance, resulting in an enhanced absorption rate of the metamaterial structure with similar changes to those of a single TiO_2 structure.

To investigate the reasons for the high absorption of the device, we

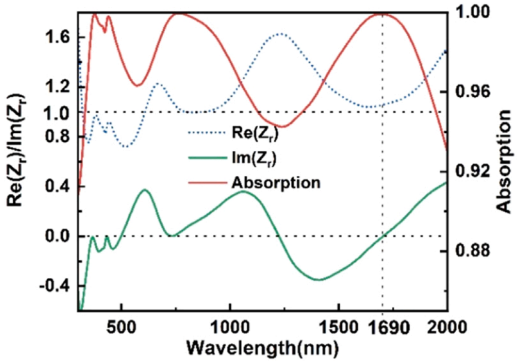

Fig. 8. Impedance and absorption of the absorber.

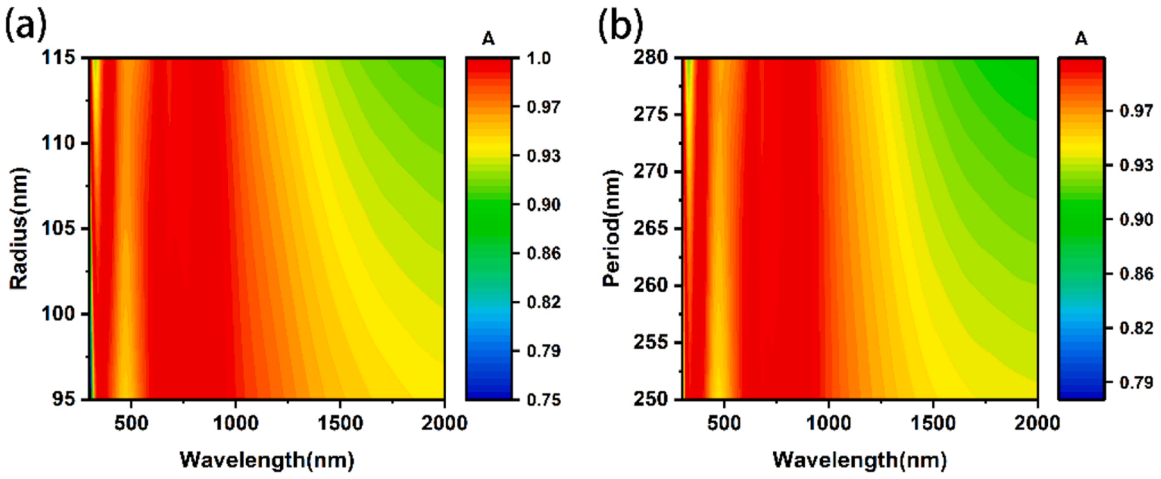

Fig. 7. (a) Evolution of absorption as the radius of the composite nanopillar changes. (b) Evolution of absorption as the period of nanopillar changes from 250 nm to 280 nm.

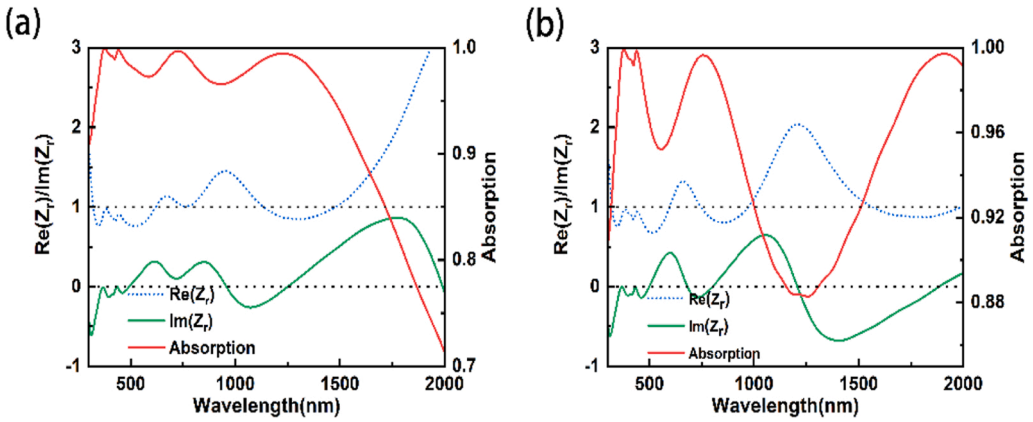

Fig. 9. Impedance and absorption curves of the proposed absorber utilizing TiN (a) and TiO_2 (b) as L_5.

calculated the absorption power density of the TiN side in the longitudinal section, as shown in Fig. 10. At a wavelength of 760 nm, the absorption power density on the surface of the titanium layer was significantly higher than that of other layers. This is mainly due to the strong absorption of light by high-density free electrons near the metal surface. When light is incident on the metal surface, free electrons near the Fermi level can absorb energy from the penetrating photons through inter-band and intra-band transitions. In addition, the collective oscillation of incident light waves and free electrons leads to the excitation of plasma resonances, such as bulk plasmon (BP), surface plasmon (SP), and localized surface plasmon (LSP). Furthermore, we found that the design of metamaterial structures can enhance the excitation of plasmon resonances (especially LSP), thereby improving the absorption efficiency [45,46]. To further elucidate the physical mechanism behind the high absorption in the metamaterial solar absorber, the longitudinal cross-sectional electric field at different wavelengths was calculated using a detector, as shown in Fig. 11. The higher electric field intensity is mainly concentrated in the transverse area of the GaP, SiO2, and Ti nanorods. In addition, as the wavelength increases, the electric field intensity on both sides of the titanium layer also increases. This can be attributed to the strong ability of titanium to generate plasmon resonances. When the relative dielectric constant and dielectric constant of the interface meet the momentum-matching requirements, surface plasmon resonance occurs at the metal-dielectric interface. The excitation of surface plasmon resonance is generated through the resonance between the free electrons on the metal surface and the incident wave,

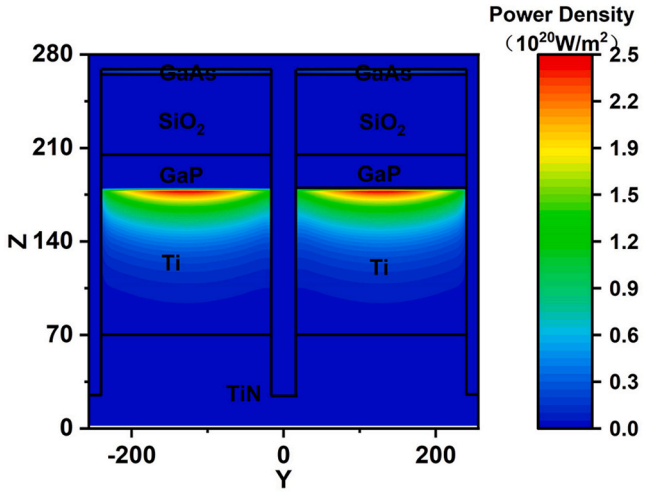

Fig. 10. Absorbed power density of Y-Z longitudinal section of the absorber at a wavelength of 760 nm.

thus producing surface plasmon excitation (SPP) in a single nanorod. The microcavities between the nanorods can also resonate, and when the resonant frequency of the incident light matches that of the microcavities, the electric field in the microcavities is significantly enhanced, thereby increasing the absorption of the device by the incident light. In addition, the presence of microcavities can further enhance the localized electric field of the device, thereby increasing the excitation and absorption efficiency of surface plasmon resonance. Therefore, the resonance of microcavities in the nanoscale structure plays an important role in the high absorption efficiency of the device.

The absorption curve of the proposed metamaterial absorber is shown in Fig. 12. When the light source is vertically incident, the average absorption of the metamaterial absorber can reach more than 97% in the wavelength of 300–2000 nm. Additionally, the absorption is close to 100% in the wavelength of 300–500 nm, 600–800 nm, and 1500–1700 nm. To verify the superiority of the designed absorber structure, the sensitivity of the device to the incident angle and polarization direction of light was subsequently calculated.

As shown in Fig. 13(a), the absorption of the device changes with the polarization angle in the wavelength range of 300–400 nm. However, the absorption of the metamaterial structure is stable in the range of 400–2000 nm, almost independent of the polarization angle. Therefore, it can be concluded that the structure is insensitive to polarization changes and still exhibits absorption of over 97% in the wavelength of 300–2000 nm. Under the condition of keeping the polarization direction constant, the effect of oblique incidence on absorption was further studied by calculating the absorption spectra at different incident angles. As shown in Fig. 13(b), the absorption ability of the structure is significantly affected by the incidence angle change. This is because the TM wave mainly induces surface plasmon excitation, and the x component of the electric field weakens with the increase of the incidence angle. As the incidence angle increases, the surface plasmon resonance effect begins to weaken. In addition, the decrease in the electric field component weakens the coupling between the cavity mode resonance and the mode. The study found that as the incidence angle increases from 0 degrees, the absorption in the long wavelength band gradually decreases. At 40 degrees of deviation, the absorption in the visible light band decreases, while the absorption in the long wavelength band increases. However, the total absorption rate still remains above 90%. These results indicate that the metamaterial absorption structure is relatively insensitive to polarization of visible light and infrared wavelengths, exhibiting the characteristics of wide-angle and high absorption, which is advantageous for light absorption.

To evaluate the absorption characteristics of the metamaterial, we analyzed the distribution of solar spectral power density absorbed using the standard solar radiation spectrum AM 1.5. As shown in Fig. 14, the black spectrum represents the standard solar radiation spectrum of AM 1.5, while the red region represents the total absorption power of the

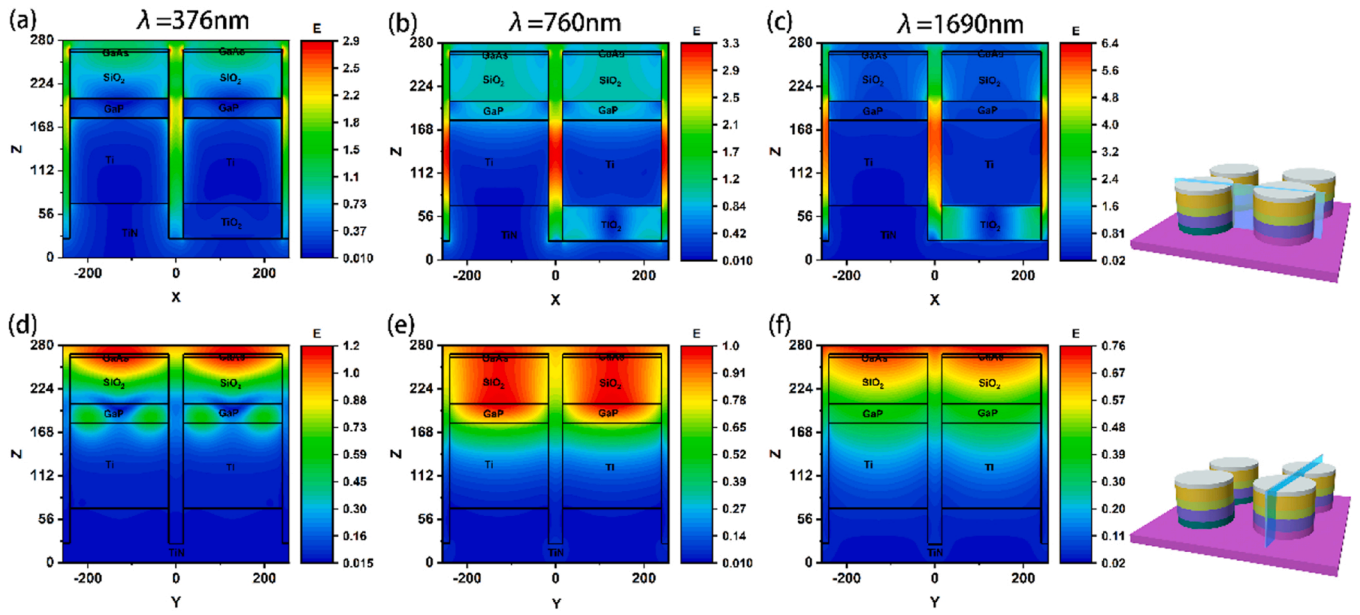

Fig. 11. Electric field distributions at 376 nm, 760 nm, and 1690 nm in the cross-sections perpendicular (a,b,c) and parallel (d,e,f) to the direction in which the nanopillar with a similar composite structure.

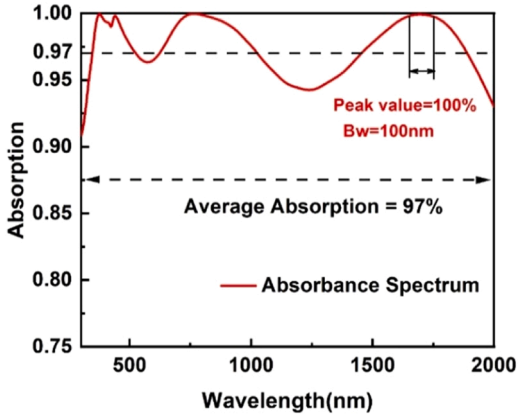

Fig. 12. Absorptance curve of the absorber with optimized structure. The absorption near 1600nm is close to 100%, with a high absorption bandwidth (Bw) of 100nm.

metamaterial. It is worth noting that only a tiny fraction of the energy is not absorbed by the absorption structure (orange region). This result indicates that the proposed metamaterial absorption structure can effectively absorb light in the wavelength range of 300 nm to 2000 nm,

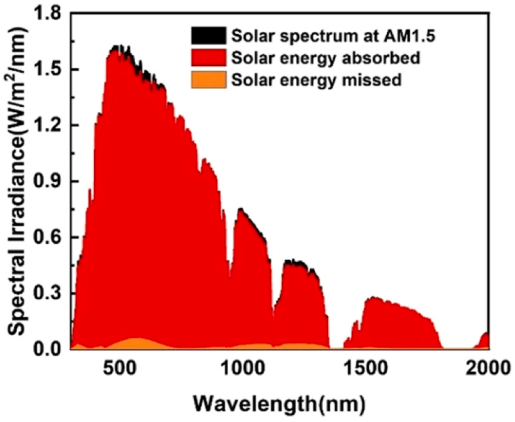

Fig. 14. The energy absorbed and lost by the absorber under AM 1.5.

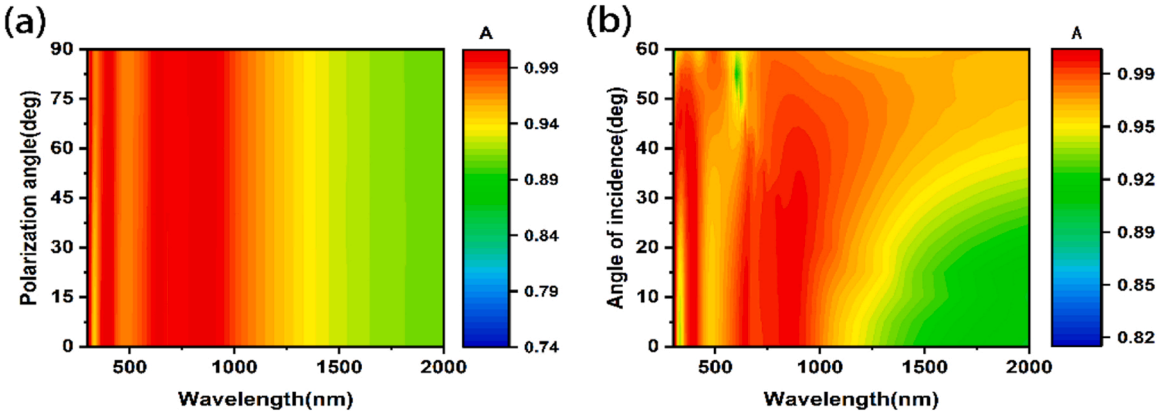

Fig. 13. 2D plot of the absorptance as the polarization (a) and incident angle (b) of the light source changes.

making it a potential candidate for energy absorption and photovoltaic system applications.

4. Conclusion

In summary, this paper proposes a metamaterial structure formed by periodic arrays of two types of interlaced nanopillars. Highly efficient absorption of the solar spectrum in a wide wavelength range from 300–2000 nm, with an average absorption efficiency of 97%, especially in the 700 nm band and 1700 nm band, where the absorption efficiency reaches 100%, achieving perfect absorption of incident light. Efficient light absorption plays a crucial role in numerous applications, such as photothermal devices, electromagnetic stealth, and stray light suppression. The simulation results demonstrate that the efficient absorption mainly comes from the side of the nanopillar titanium and gallium phosphide layers. Furthermore, the absorber with periodically arranged nanopillar array structure shows insensitivity to the angle of light incidence and polarization direction, with an average absorption efficiency above 90% as the angle increases from 0° to 90°. In addition, the analysis of the electric field distribution and impedance characteristics of the interlaced nanopillar periodic units at different wavelengths reveals that the electromagnetic properties of the selected materials and the physical properties of the structures are the main reasons for achieving high absorption of the structures at wide wavelengths. The interleaved arrangement of several nanopillar array structures with different absorption properties can form a linear superposition of incident light absorption. Moreover, the micro-cavity feature between the nanopillar arrays allows for adjusting the appropriate resonance wavelength, which helps achieve high absorption characteristics at a wide range of wavelengths. This work provides a novel approach for the design of broad-band near-perfect absorption structures and a feasible way to meet the demands of efficient photothermal devices, electromagnetic stealth, and stray light suppression.

Declaration of Competing Interest

The authors declare that they have no known competing financial interests or personal relationships that could have appeared to influence the work reported in this paper.

Data Availability

The data presented in this study are available on request from the corresponding author.

Acknowledgments

This research was funded by Open funding of the State Key Laboratory of Applied Optics in Changchun Institute of Optics of the Chinese Academy of Sciences, grant number SKLAO2021001A09. Young Science and Technology Talent Cultivation Project of China Jiliang University (Grant Number 2022YW57).

References

[1] J. Valentine, S. Zhang, T. Zentgraf, et al., Three-dimensional optical metamaterial with a negative refractive index, Nature 455 (7211) (2008) 376–379.
[2] J. Xu, J. Cao, M. Guo, et al., Metamaterial mechanical antenna for very low-frequency wireless communication, Adv. Compos. Hybrid Mater. 4 (3) (2021) 761–767.
[3] P. Segovia, G. Marino, A.V. Krasavin, et al., Hyperbolic metamaterial antenna for second-harmonic generation tomography, Opt. Express 23 (24) (2015) 30730–30738.
[4] D. Shin, Y. Urzhumov, Y. Jung, et al., Broadband electromagnetic cloaking with smart metamaterials, Nat. Commun. 3 (1) (2012) 1213.
[5] X. Ni, Z.J. Wong, M. Mrejen, et al., An ultrathin invisibility skin cloak for visible light, Science 349 (6254) (2015) 1310–1314.
[6] D. Li, Z. Szabó, X. Qing, et al., A high gain antenna with an optimized metamaterial inspired superstrate, IEEE Trans. Antennas Propag. 60 (12) (2012) 6018–6023.
[7] P. Mookie, K.R. Dandekar, Metamaterial-substrate antenna array for MIMO communication system, IEEE Trans. Antennas Propag. 57 (10) (2009) 3283–3292.
[8] N.I. Landy, S. Sajuyigbe, J.J. Mock, et al., Perfect metamaterial absorber, Phys. Rev. Lett. 100 (20) (2008), 207402.
[9] J. Zhang, G. Wang, B. Zhang, et al., Photo-excited broadband tunable terahertz metamaterial absorber, Opt. Mater. 54 (2016) 32–36.
[10] Chuan Li, Zhongyin Xiao, Xinyan Ling, Xiaoxia Zheng, Broadband visible metamaterial absorber based on a three-dimensional structure, Waves Random Complex Media 29 (3) (2019).
[11] M. Nejat, N.Design Nozhat, theory, and circuit model of wideband, tunable and polarization-insensitive - 6 -terahertz absorber based on graphene, IEEE Trans. Nanotechnol. 18 (2019) 684–690.
[12] J. Cong, Z. Zhou, B. Yun, et al., Broadband visible-light absorber via hybridization of propagating surface plasmon, Opt. Lett. 41 (9) (2016) 1965–1968.
[13] N.T.Q. Hoa, P.H. Lam, P.D. Tung, et al., Numerical study of a wide-angle and polarization-insensitive ultra-broadband metamaterial absorber in the visible and near-infrared region, IEEE Photonics J. 11 (1) (2019) 1–8.
[14] D. Wu, C. Liu, Y. Liu, et al., Numerical study of a wide-angle polarization-independent ultra-broadband efficient selective metamaterial absorber for near-ideal solar thermal energy conversion, RSC Adv. 8 (38) (2018) 21054–21064.
[15] Z. Yi, J. Li, J. Lin, et al., Broadband polarization-insensitive and wide-angle solar energy absorber based on tungsten ring-disc array, Nanoscale 12 (45) (2020) 23077–23083.
[16] R.A. Pala, J. White, E. Barnard, et al., Design of plasmonic thin-film solar cells with broadband absorption enhancements, Adv. Mater. 21 (34) (2009) 3504–3509.
[17] O. Stenzel, A. Stendal, K. Voigtsberger, et al., Enhancement of the photovoltaic conversion efficiency of copper phthalocyanine thin film devices by incorporation of metal clusters, Sol. Energy Mater. Sol. Cells 37 (3–4) (1995) 337–348.
[18] Z. Liu, P. Tang, X. Liu, et al., Truncated titanium/semiconductor cones for wide-band solar absorbers, Nanotechnology 30 (30) (2019), 305203.
[19] F. Qin, X. Chen, Z. Yi, et al., Ultra-broadband and wide-angle perfect solar absorber based on TiN nanodisk and Ti thin film structure, Sol. Energy Mater. Sol. Cells 211 (2020), 110535.
[20] J. Pflüger, J. Fink, Determination of optical constants by high-energy, electron-energy-loss spectroscopy (EELS)[M]//Handbook of Optical Constants of Solids, Academic Press, 1997, pp. 293–311.
[21] J. Pflüger, J. Fink, W. Weber, et al., Dielectric properties of TiC x, TiN x, VC x, and VN x from 1.5 to 40 eV determined by electron-energy-loss spectroscopy, Phys. Rev. B 30 (3) (1984) 1155.
[22] Ghosh G. Dispersion-equation coefficients for the refractive index and birefringence of calcite and quartz crystals[J]. Optics communications, 1999, 163 (1–3): 95–102.P. B. Johnson and R. W. Christy. Optical constants of transition metals: Ti, V, Cr, Mn, Fe, Co, Ni, and Pd, Phys. Rev, 1974: B 9, 5056–5070.
[23] W. Li, U. Guler, N. Kinsey, et al., Refractory plasmonics with titanium nitride: broadband metamaterial absorber, Adv. Mater. 26 (47) (2014) 7959–7965.
[24] P.B. Johnson, R.W. Christy, Optical constants of transition metals: Ti, v, cr, mn, fe, co, ni, and pd, Phys. Rev. B 9 (12) (1974) 5056.
[25] S. Adachi, Optical dispersion relations for GaP, GaAs, GaSb, InP, InAs, InSb, Al x Ga1− x As, and In1− x Ga x As y P1− y, J. Appl. Phys. 66 (12) (1989) 6030–6040.
[26] D.E. Aspnes, S.M. Kelso, R.A. Logan, et al., Optical properties of Al x Ga1− x As, J. Appl. Phys. 60 (2) (1986) 754–767.
[27] D.E. Aspnes, A.A. Studna, Dielectric functions and optical parameters of si, ge, gap, gaas, gasb, inp, inas, and insb from 1.5 to 6.0 ev, Phys. Rev. B 27 (2) (1983) 985.
[28] J.R. DeVore, Refractive indices of rutile and sphalerite, JOSA 41 (6) (1951) 416–419.
[29] F. Ding, J. Dai, Y. Chen, et al., Broadband near-infrared metamaterial absorbers utilizing highly lossy metals, Sci. Rep. 6 (1) (2016) 1–9.
[30] M. Melli, M. West, S. Hickman, et al., Gallium phosphide optical metasurfaces for visible light applications, Sci. Rep. 10 (1) (2020) 20694.
[31] D.R. Gibson, E.M. Waddell, J.W. Kerr, et al., Ultradurable Phosphide-based Antireflection Coatings for Sand and Rain Erosion Protection[C]//Window and Dome Technologies and Materials III, 1760, SPIE, 1992, pp. 178–200.
[32] T.V. Teperik, F.J. García de Abajo, A.G. Borisov, et al., Omnidirectional absorption in nanostructured metal surfaces, Nat. Photonics 2 (5) (2008) 299–301.
[33] X. Xiong, S.C. Jiang, Y.H. Hu, et al., Structured metal film as a perfect absorber, Adv. Mater. 25 (29) (2013) 3994–4000.
[34] U. Guler, A. Boltasseva, V.M. Shalaev, Refractory plasmonics, Science 344 (6181) (2014) 263–264.
[35] W. Wang, Y. Qu, K. Du, et al., Broadband optical absorption based on single-sized metal-dielectric-metal plasmonic nanostructures with high-ε ″metals, Appl. Phys. Lett. 110 (10) (2017), 101101.
[36] Z. Liu, H. Zhong, G. Liu, et al., Multi-resonant refractory prismoid for full-spectrum solar energy perfect absorbers, Opt. Express 28 (21) (2020) 31763–31774.
[37] Yangping Li, Zhengtang Liu, Properties of gallium phosphide thick films prepared on zinc sulfide substrates by radio-frequency magnetron sputtering, J. Mater. Sci. Technol. 26 (2010) 1.
[38] A. Tittl, M.G. Harats, R. Walter, et al., Quantitative angle-resolved small-spot reflectance measurements on plasmonic perfect absorbers: impedance matching and disorder effects, Acs Nano 8 (10) (2014) 10885–10892.
[39] W. Li, U. Guler, N. Kinsey, et al., Refractory plasmonics with titanium nitride: broadband metamaterial absorber, Adv. Mater. 26 (47) (2014) 7959–7965.
[40] Z. Liu, G. Liu, Z. Huang, et al., Ultra-broadband perfect solar absorber by an ultra-thin refractory titanium nitride meta-surface, Sol. Energy Mater. Sol. Cells 179 (2018) 346–352.

[41] M.M.K. Shuvo, M.I. Hossain, S. Mahmud, et al., Polarization and angular insensitive bendable metamaterial absorber for UV to NIR range, Sci. Rep. 12 (1) (2022) 4857.
[42] D.R. Smith, R. Dalichaouch, N. Kroll, et al., Photonic band structure and defects in one and two dimensions, J. Opt. Soc. Am. B 10 (2) (1993) 314–321.
[43] P. Yu, L.V. Besteiro, Y. Huang, et al., Broadband metamaterial absorbers, Adv. Opt. Mater. 7 (3) (2019) 1800995.
[44] M.A. Awad, A.H. Aly, Experimental and theoretical studies of hybrid multifunctional TiO_2/TiN/TiO_2, Ceram. Int. 45 (15) (2019) 19036–19043.
[45] H. Gong, X. Liu, G. Liu, et al., Non-noble metal based broadband photothermal absorbers for cost effective interfacial solar thermal conversion, Nanophotonics 9 (6) (2020) 1539–1546.
[46] Y. Wang, H. Ma, J. Yu, et al., All-dielectric insulated 3D plasmonic nanoparticles for enhanced self-floating solar evaporation under one sun, Adv. Opt. Mater. (2023) 2201907.